LOGIC
Journal of Engineering Design and Technology
Vol. 26 No. 1 March 2026 ; p. 86 - 94

p-ISSN : 1412-114X
e-ISSN : 2580-5649
http://ojs2.pnb.ac.id/index.php/LOGIC

NUMERICAL STUDY ON THERMAL PERFORMANCE OF MINI-CHANNEL COOLING ON CYLINDRICAL LITHIUM-ION BATTERY COOLING SYSTEM

Elvi Armadani[1], James Julian[2)*], Bima Rakha Adhitama[2)], Fitri Wahyuni[2)], Riki Hendra Purba[2)], Fathin Muhammad Mahdhudhu[3)], Adi Winarta[4)]

1) Industrial Engineering, Universitas Pembangunan
2) Mechanical Engineering, Universitas Pembangunan Nasional Veteran Jakarta
3) Naval Architecture, Universitas Pembangunan Nasional Veteran Jakarta
4) Mechanical Engineering, Politeknik Negeri Bali

Corresponding email [1)] : zames@upnvj.ac.id

Abstract. This study numerically examines the effect of liquid-based cooling on the thermal performance of a cylindrical lithium-ion battery pack under a 5C discharge rate. Proper thermal management is essential to ensure safety and extend battery life, particularly in electric vehicle applications. Three cooling-channel diameters (4, 6, and 8 *mm*) were evaluated. The 8 *mm* channel achieved the best thermal performance, with a maximum temperature of 36.2 °C and a average temperature of 33.6 °C. In contrast, the 4 *mm* channel reached 37.8 °C and produced the highest temperature gradient (8.3 °C), increasing hotspot risk. Pressure drop analysis revealed that the 4 *mm* configuration had the greatest hydraulic resistance, while 6 *mm* and 8 *mm* channels reduced ΔP by 28% and 46%, respectively. Overall, an 8 *mm* diameter provides optimal thermal uniformity and lower pumping power requirements.

Keywords : Hotspot, Li-ion battery, Liquid coooling

1. INTRODUCTION

Transportation is widely acknowledged as a major sector responsible for producing greenhouse gas emissions and contributing to deteriorating air quality in urban regions [1]. To address these issues and reduce reliance on petroleum-based fuels, the transition from conventional internal combustion vehicles to Electric Vehicles (EVs) has been increasingly advocated [1]. Lithium-ion batteries (LIB) are predominantly selected as the main energy-storage component for EVs because they possess several advantageous characteristics, including high energy density, strong power capability, extended lifespan, low self-discharge behavior, and the absence of memory effects [2]. Even so, the heat generated during charge–discharge processes can elevate the cell temperature, consequently influencing the battery's cycle durability, performance consistency, reliability, and safety [3]. If the temperature rise becomes excessive, the battery may experience hazardous events such as thermal runaway [3]. Prior investigations have indicated that lithium-ion batteries should ideally operate within a temperature window of approximately 20 °C to 40 °C, while the allowable temperature difference across the battery is recommended to remain below about 5°C [4]. This thermal control can be applied either within individual cells or across battery modules [4].

Therefore, establishing an effective battery thermal-management approach is essential. Cooling methodologies are generally categorized based on the medium involved, including air cooling [5][6], liquid cooling [7][8], heat-pipe systems [9][10], phase-change-material (PCM) cooling [11][12], and hybrid methods [13]. Among these options, air cooling is often considered the simplest technique, where airflow is directed into the battery structure using devices such as fans to enhance heat removal. Various studies have attempted to improve air-cooling performance by adjusting the airflow distribution. Yang et al. [14], for instance, demonstrated that changes in inlet angle affect the resulting airflow patterns. Additional parameters such as cell arrangement, spacing between cells, and airflow velocity have also been explored. Nonetheless, air cooling becomes less suitable for modern high-rate charge scenarios due to its inherently limited thermal-conductivity capability. Conversely, PCM-based cooling offers the advantage of reducing temperature and maintaining a low temperature gradient, although its application is restricted by the material's thermal properties and melting characteristics. Meanwhile, liquid cooling has been identified as the most effective BTMS method [15] with maximum temperature reductions of 8–14 °C and ΔT maintained within 3–5 °C [16] but its use remains constrained by structural complexity, and pumping

power requirements.

This study focuses on evaluating the thermal performance of a liquid cooling system applied to cylindrical Li-ion battery packs consisting of eight cells. The research emphasizes the importance of energy efficiency, where the cooling method is expected not only to dissipate the internal heat generated during charge and discharge but also to minimize additional energy consumption. Numerical simulations are employed to analyze the effect of cold plate design variations, particularly through the use of internal channels with different inlet diameters. By maximizing the contact area between the cooling surface and the battery, these variations are proposed to improve overall uniformity across the battery pack. Furthermore, the study provides insights into enhancing both thermal safety and operational efficiency in LIB battery packs.

2. RESEARCH METHODS

2.1 Geometry of the Models

To evaluate the influence of cooling channel dimensions on the thermal performance of the battery pack, three geometric variations of the liquid cold plate were designed. Each model integrates cylindrical Li-ion cells with embedded cooling channels, allowing water to circulate and remove the generated heat. The variations are the cooling channel, where diameters were set to 4 *mm*, 6 *mm*, and 8 *mm*. The corresponding layouts of these designs are illustrated in figure 1. Specifically, model (a) represents the 4 *mm* channel configuration, model (b) corresponds to the 6 *mm* channel, and model (c) illustrates the 8 *mm* channel. These configurations were developed to investigate the relationship between channel diameter, temperature uniformity, and heat dissipation efficiency across the battery pack.

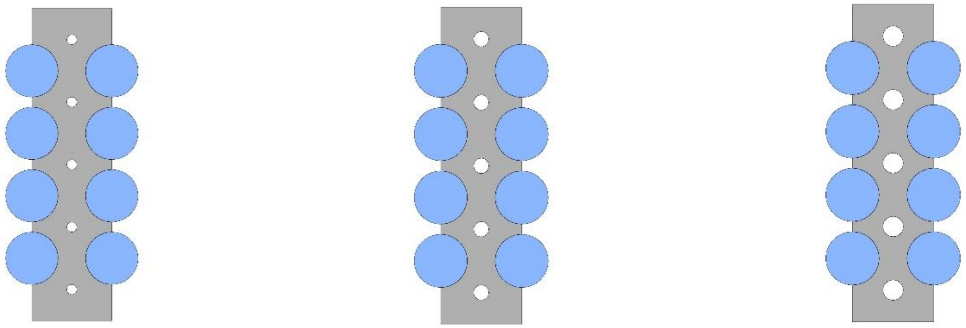

(a) (b) (c)

Figure 1. (a) 2-D view of the 4 *mm* channel on the LIBs pack, (b) 2-D view of the 6 *mm* channel on the LIBs pack, (c) 2-D view of the 8 *mm* channel on the LIBs pack

2.2 Governing Equations

To evaluate the cooling behavior of the battery system, the analysis first addresses the fluid-flow characteristics by employing the Reynolds-Averaged Navier–Stokes (RANS) formulation for mass and momentum conservation, as presented in Eq. 1 and 2 [17]. The subsequent thermal response of the battery is then described through the energy-balance relation in Eq. 3, with a heat source model based on experimental thermal characteristics at Eq. 4. This model is further developed into a parametric function in Eq. 5. The parametric coefficient was set based on Z. Rao experiment [23], representing the vertical heat inhomogeneity observed experimentally. The function was implemented in numerical software as a spatially dependent volumetric heat source using a UDF [18], [19], [20], [21]. These governing equations provide the model which ensures that the cooling channel configurations can be systematically assessed for their impact on maximum temperature, temperature uniformity, and overall thermal efficiency. [21]

$$\frac{\partial \rho}{\partial t} + \frac{\partial}{\partial x_i}(\rho u_i) = 0 \quad (1)$$

$$\frac{\partial}{\partial t}(\rho u_i) + \frac{\partial}{\partial x_i}(\rho u_i u_j) = \frac{\partial p}{\partial x_i} + \frac{\partial}{\partial x_j}\left[\mu\left(\frac{\partial u_i}{\partial x_j} + \frac{\partial u_j}{\partial x_i} - \frac{2}{3}\delta_{ij}\frac{\partial u_i}{\partial x_i}\right)\right] + \frac{\partial}{\partial x_i}\left(-\rho\overline{u_i' u_j'}\right) \quad (2)$$

$$\rho c_p \frac{\partial T}{\partial t} = \lambda_x \frac{\partial^2 T}{\partial^2 x} + \lambda y \frac{\partial^2 T}{\partial^2 y} + \lambda z \frac{\partial^2 T}{\partial^2 z} + Q_{gen} \quad (3)$$

$$Q_{gen}(t) = \rho c_p \frac{\Delta T}{\Delta t} \quad (4)$$

$$Q_{gen(1-3)}(x,y,z,t) = Q_{gen(1-3)}(t) - \lambda \nabla^2 T_{(1-3)} \quad (5)$$

2.3 Mesh and Boundary Conditions

To effectively capture the complex geometry of the battery cooling system, the computational domain was discretized using an unstructured tetrahedral mesh. This meshing strategy offers flexibility and accurate representation of faces at the cylindrical cells. Figure 2(a) illustrates a schematic of the liquid cooling system of the battery module, while figure 2(b) presents the mesh distribution. The system is composed of cylindrical cells embedded in an aluminum block, which incorporates five liquid coolant channels. The inlet mass flow rate was set to 0.0035 kg/s remembering pump power consumption. Velocity-inlet conditions were applied at the inlets, while a no-slip condition was applied on the internal channel surfaces. The entire module was assumed to be adiabatic, with an inlet liquid temperature fixed at 25 °C. The material properties employed in the simulation showed in Table 1.

Table 1. Material Properties

Materials	ρ ($kg \cdot m^{-3}$)	C ($J \cdot kg^{-1} \cdot k^{-1}$)	k ($W \cdot m^{-1} \cdot k^{-1}$)	μ ($g\, m^{-1}\, s^{-1}$)
Aluminum	2719	871	202.4	-
Battery	2450	1108.4	3.917	-
Water	998.2	4128	0.6	1.003

(a) (b)

Figure 2. (a) Boundary conditions (b) Mesh

2.4 Grid Independence Test

The accuracy of Computational Fluid Dynamics (CFD) simulations is strongly influenced by the quality of the mesh employed. To ensure reliable model, a grid independence test was carried out using different meshes, where the coarse mesh consisted of 1,555×106 elements, the medium mesh of 2.333×106 elements, and the fine mesh of 3,5E×106 elements. The Richardson extrapolation technique, generalized by Roache [22], was applied as the methodological basis. Equations (9) and (10) were utilized to estimate the numerical error for both coarse and fine mesh cases, while a safety factor of 1.25 was adopted. The relative error values obtained, as presented in Table 2, indicated that mesh refinement affected the convergence index. As illustrated in figure 3, higher mesh resolution was associated with improved accuracy. Therefore, the fine mesh configuration was selected for subsequent simulations.

$$r = \frac{h_2}{h_1} \quad (7)$$

$$\bar{p} = \frac{\ln\left(\frac{f_3 - f_2}{f_2 - f_1}\right)}{\ln(r)} \quad (8)$$

$$GCI_{fine} = \frac{F_s \,|\in|}{\left(r^{\bar{p}} - 1\right)} \tag{9}$$

$$GCI_{coarse} = \frac{F_s \,|\in| \, r^{\bar{p}}}{\left(r^{\bar{p}} - 1\right)} \tag{10}$$

$$\in = \frac{f_{n+1} - f_n}{f_n} \tag{11}$$

$$\frac{GCI_{coarse}}{GCI_{fine} r^{\bar{p}}} \approx 1 \tag{12}$$

$$f\,\mathrm{r}_{h=0} = f_1 + \frac{(f_1 - f_2)}{\left(r^{\bar{p}} - 1\right)} \tag{13}$$

Table 2. Result of grid convergence index

Mesh	Fine	Medium	Coarse
Difference of Temperature	35.1710	35.10881	34.82375
p"		3.751619273	
R		1.5	
GCI_{fine}		0.0062%	
GCI_{coarse}		0.2837%	
$f_{rh}= 0$		35.1884	
$\frac{GCI_{coarse}}{GCI_{fine}^{p"}}$		1	
Error	0.04947%	0.22644%	1.03654%

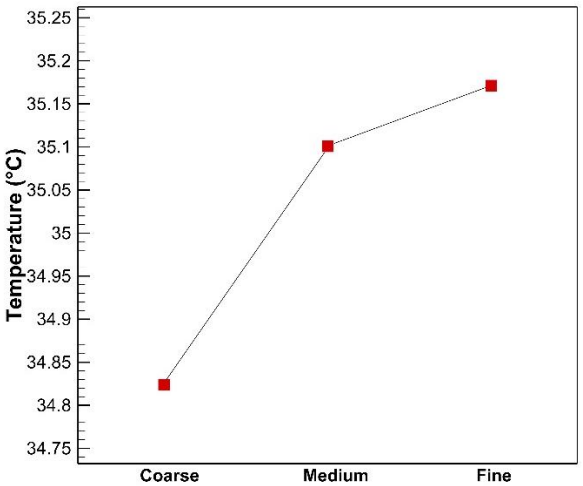

Figure 3. Mesh Sensitivity

3. RESULTS AND DISCUSSION

3.1 Validation

The experimental data utilized were obtained from the values of three heat sources who conducted by Z. Rao et. al. [23]. The setup conducted in such a way as to account for the slightly larger chemical reaction occurring at the positive terminal compared to other regions. The primary objective was the capture of vertical inhomogeneity within the battery. The experiment was performed at a discharge rate of 5C, representing high-power operating conditions in which thermal effects are more significant and critical for performance evaluation. As illustrated in figure 4, the predicted temperature closely matched the experimental data, with a maximum deviation of only 3.99%, which validates the suitability of the heat-generation model adopted in this study.

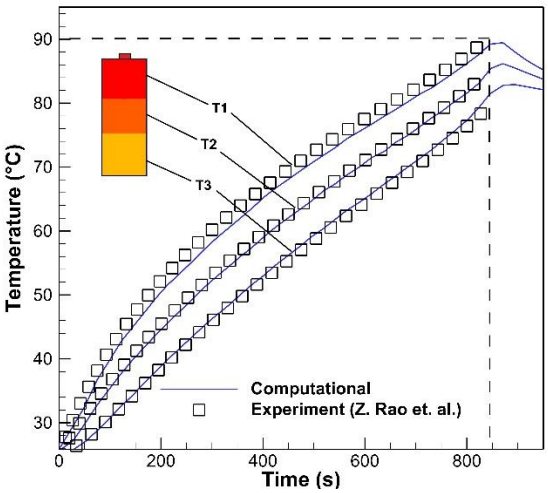

Figure 4. Validation with experiment

3.2 Analysis

Figure 5 presents the maximum temperature distribution of the battery pack for three cooling channel diameters, elucidating the influence of channel geometry on peak thermal management. In each scenario, the temperature profile initiates at 25 °C and exhibits a pronounced increase within the initial 200–300 s, subsequently followed by a gradual decline as the coolant counteracts the heat produced by internal electrochemical reactions. This transient response underscores the interplay between heat generation during 5C discharge and the thermal dissipation capacity of the liquid cooling architecture. For the *Ø4mm* configuration, the maximum temperature attains approximately 37.8 °C, representing the highest value among the three cases. The pronounced slope from 0 to 300 s reflects the restricted channel diameter, which limits coolant flow and diminishes the convective heat transfer coefficient. Consequently, thermal energy accumulates rapidly, resulting in an increased temperature gradient across the cells. Even after reaching quasi-steady-state, the temperature remains elevated at approximately 35°C, signifying suboptimal mitigation of peak thermal loads. The *Ø6mm* channel exhibits improved thermal performance, with the maximum temperature reduced to 36.9 °C.

The transient temperature rise retains an exponential character but with a diminished gradient relative to the 4mm case, indicating a more equilibrated relationship between heat generation and dissipation. The stabilized temperature decreases to approximately 34.2°C, constituting a moderate yet significant improvement in cooling efficiency. This configuration represents a balance between hydraulic resistance and effective thermal management. The *Ø8mm* channel achieves the most effective thermal management, constraining the maximum temperature to approximately 36.2 °C and stabilizing at 33.6 °C. The temperature profile within the initial 0–300 s is comparatively smoother, reflecting the superior efficacy of the enlarged flow passage in mitigating thermal accumulation. This configuration not only attenuates the overall peak temperature but also facilitates more rapid stabilization, thereby minimizing the likelihood of localized thermal hotspots. Across all configurations, the nearly superimposed temperature curves among the cells indicate a symmetrical coolant distribution. Nonetheless, smaller channel diameters yield increased peak gradients and a delayed thermal response. By contrast, the *Ø8mm* channel consistently exhibits enhanced cooling capacity, improved system stability, and superior safety margins under high-power operating conditions.

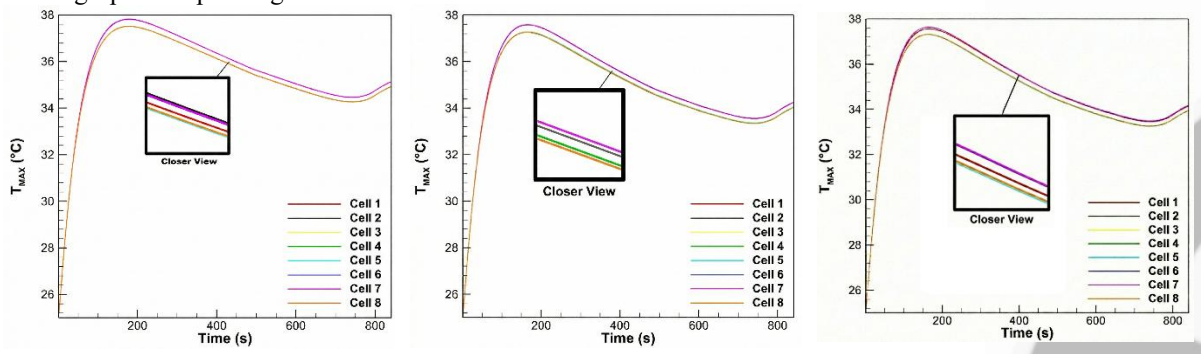

(a) (b) (c)

Figure 5. (a) Max temp. *Ø4mm* (b) Max temp. *Ø6mm* (c) Max temp. *Ø8mm*

Figure 6 presents the ΔT (temperature difference) curves for channel diameters of 4, 6, and 8 *mm*, illustrating the significance of temperature uniformity within the battery pack. All investigated configurations display a pronounced increase in temperature difference during the initial stage of discharge (0–200 s), corresponding to a

period when heat generation exceeds heat dissipation. Following the peak, ΔT progressively declines as the temperature distribution among the cells approaches steady state. For the 4 *mm* channel diameter, the maximum ΔT attains 8.3 °C, the largest among the examined cases. The reduced channel dimension limits coolant flow, resulting in non-uniform heat extraction across the cells. This condition leads to the formation of localized hot spots, with cells at suboptimal cooling positions exhibiting elevated temperatures. Pronounced temperature gradients accelerate degradation mechanisms, shorten cycle life, and increase the likelihood of thermal runaway. The 6 *mm* channel demonstrates enhanced temperature uniformity.

The increased cross-sectional area facilitates improved coolant circulation, promoting more homogeneous heat removal from the cells. Although minor discrepancies persist between individual cells, the decrease in ΔT signifies a notable enhancement in thermal safety. The 8 *mm* channel achieves the most uniform temperature distribution, as ΔT is minimized. The temperature profiles of all eight cells exhibit greater overlap, indicating that heat dissipation is consistently maintained throughout the module. The smoother gradient observed during the transient phase suggests that the system effectively balances heat generation and removal, thereby limiting the development of thermal gradients. Maintaining temperature uniformity is essential for the safety and optimal performance of lithium-ion batteries. Even minor ΔT values between cells can induce non-uniform aging, with hotter cells undergoing accelerated degradation, thereby reducing the overall module capacity and lifespan. Consequently, minimizing ΔT through optimized cooling design not only enhances operational safety but also promotes long-term reliability and energy efficiency of the battery pack.

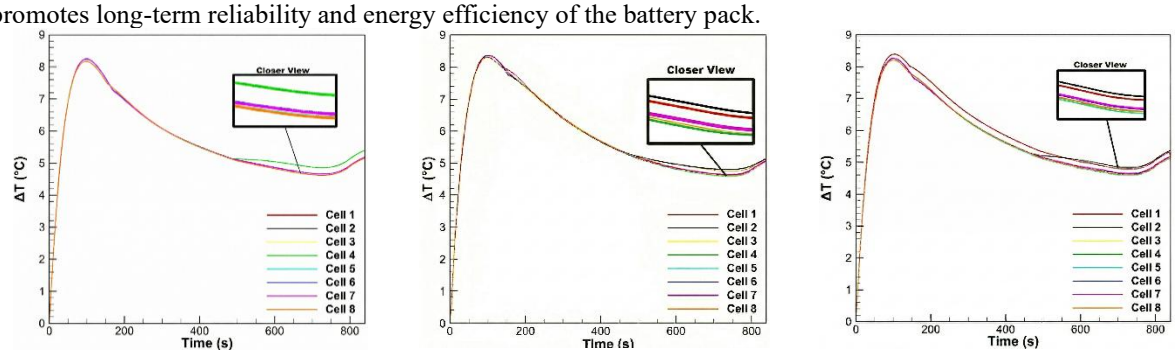

(a) (b) (c)

Figure 6. (a) ΔT *Ø4mm* (b) ΔT *Ø6mm* (c) ΔT *Ø8mm*

Table 3 presents the reduction of thermal difference for each battery cell under different cooling channel diameters of 4, 6, and 8 *mm*, compared to the baseline condition without cooling. In the no-cooling case, the maximum ΔT across the module was recorded at 59.358 °C. With the implementation of liquid cooling, all configurations demonstrate a remarkable reduction in ΔT exceeding 85%, confirming the effectiveness of channel-based cooling in suppressing temperature gradients among the cells. Specifically, the 4 *mm* channel yields an average ΔT reduction of 86.092%, the 6 *mm* channel achieves 86.108%, and the 8 *mm* channel records the highest improvement at 86.171%. The trend indicates that increasing channel diameter consistently enhances heat dissipation and promotes better thermal uniformity. It is also noteworthy that the reduction percentages remain stable across all eight cells, with only marginal variation between them. This indicates that the cooling system provides a nearly uniform cooling effect regardless of cell position, which is particularly important in cylindrical battery packs where localized hotspots are a critical issue. The slightly superior performance of the 8 *mm* configuration can be attributed to the larger conductive surface area and increased coolant flow capacity, which together improve the heat transfer rate from the cells to the coolant.

Table 3. Thermal difference reduction

Cell	No Cooling	*4mm*	*6mm*	*8mm*
	ΔT (°C)	ΔT reduction (%)	ΔT reduction (%)	ΔT reduction (%)
1	59.358	85.859	86.155	86.230
2		86.093	86.051	86.107
3		86.086	86.063	86.108
4		86.172	86.160	86.235
5		86.176	86.159	86.237
6		86.080	86.065	86.106
7		86.092	86.053	86.116
8		86.177	86.153	86.230
Average (%)		86.092	86.108	86.171

Figure 7 presents the pressure drop (ΔP) across the cooling channel for the three investigated diameters. The results demonstrate a clear inverse relationship between channel diameter and pressure drop. This trend is attributed to the reduction in hydraulic resistance as the channel area increases. A larger diameter reduces flow velocity and

wall shear stress, thereby minimizing frictional losses along the channel. From an operational perspective, lower pressure drop directly translates into reduced pumping power requirements. Notably, the *Ø8mm* configuration not only provides the best thermal performance, but also results in the lowest hydraulic resistance.

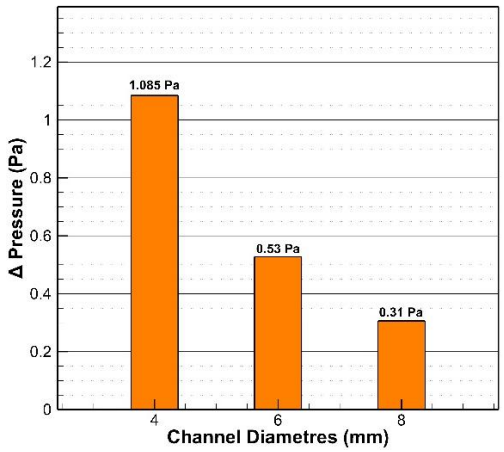

Figure 7. ΔP throughout the cooling channel

Figure 8 presents the temperature contours of the battery module under three cooling channel diameters, emphasizing the role of channel size in promoting thermal equalization and mitigating localized hotspots. At *Ø4mm* which is presented in figure 8(a), pronounced hotspot regions are observed around the mid-height of several cells, indicating localized heat accumulation and insufficient thermal dispersion. The narrow channel restricts coolant distribution, thereby limiting conduction–convection coupling and resulting in uneven temperature fields, as further evidenced by the non-uniform isothermal bands at the outlet. With an enlarged channel of *Ø6mm* presented in figure 8(b), these hotspots are significantly suppressed, and the contour distribution evolves into smoother transitions. This improvement reflects enhanced conductive spreading within the cold plate and a more effective convective heat transfer, which jointly facilitates inter-cell temperature homogenization. The *Ø8mm* configuration in figure 8(c) demonstrates the highest level of uniformity, where hotspot regions minimize consistently from inlet to outlet, and parallel contour spacing indicates a nearly isothermal module. This condition reveals that the increased channel diameter maximizes the heat removal performance, promotes more uniform gradient, and elevates the capacity for both conductive and convective dissipation. Importantly, the near elimination of localized high-temperature zones suggests a substantial improvement in thermal reliability and operational safety. Collectively, the results highlight that the enlargement of cooling channels progressively strengthens thermal equalization across the module. While *Ø6mm* offers a balanced trade-off between temperature uniformity and flow resistance, *Ø8mm* establishes itself as the optimal configuration for avoiding hotspots and ensuring stable temperature distribution, which are critical for extending the lifespan and safety of cylindrical Li-ion battery packs.

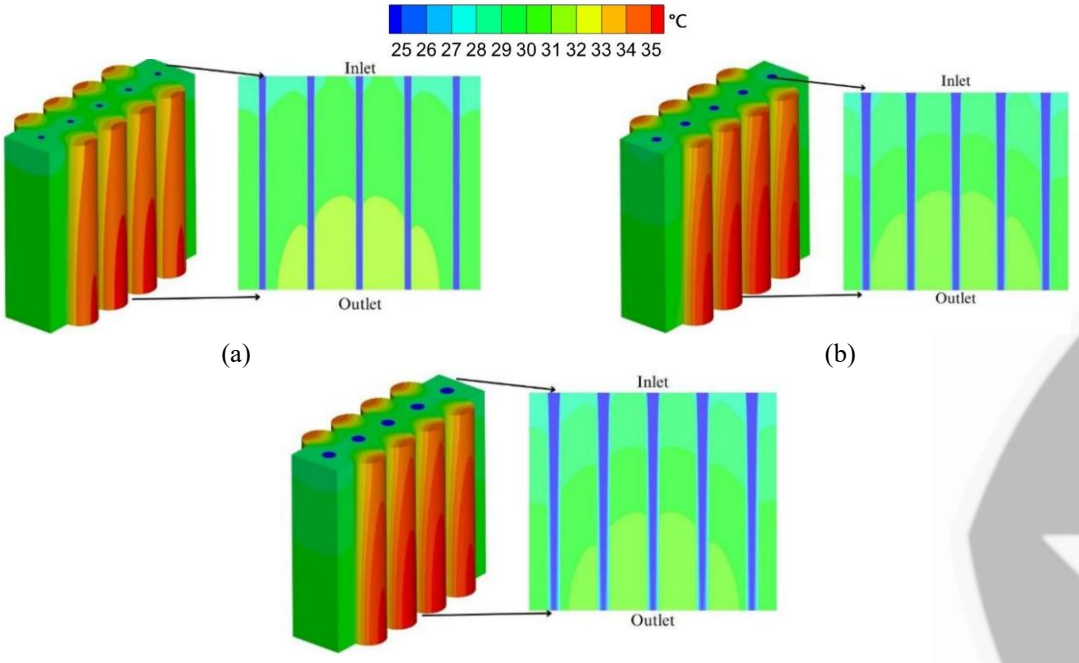

Figure 8. (a) Contour at *Ø4mm* (b) Contour at *Ø6mm* (c) Contour at *Ø8mm*

4. CONCLUSION

This study numerically evaluated the thermal performance of a liquid cooling system for a cylindrical lithium-ion (Li-ion) battery pack, focusing on the effect of cooling channel diameter. Using CFD, three configurations with channel diameters of 4 *mm*, 6 *mm*, and 8 *mm* were analyzed under a high-power 5C discharge rate. The results consistently demonstrate that the channel diameter is a critical parameter for effective thermal management. The *Ø8mm* channel configuration proved to be the most effective, achieving the lowest peak and stabilized temperatures and promoting optimal temperature uniformity across the battery cells. This superior performance is due to the larger channel size, which decreases flow resistance, enhances coolant circulation, and improves heat transfer efficiency, thereby mitigating the accumulation of thermal energy. In contrast, the *Ø4mm* and *Ø6mm* channel configurations, while still providing significant temperature reduction compared to the uncooled state, were less effective. The smaller 4 *mm* channels led to higher peak temperatures, slower thermal stabilization, and a greater temperature difference (ΔT) of 8.3 °C across the cells. This non-uniformity creates localized hotspots, which can accelerate battery degradation and increase the risk of thermal runaway. In conclusion, optimizing cooling channel diameter is essential for maintaining the operational safety, performance, and longevity of Li-ion battery packs. The findings confirm that a larger channel diameter, such as the *Ø8mm* configuration, provides a substantial advantage in mitigating thermal stress and ensuring stable, uniform temperature distribution, which is crucial for high-power applications. Future research could explore the trade-offs between pumping power requirements and thermal performance for various channel geometries to further optimize battery thermal management systems.

5. REFERENCES

[1] S. Panchal, I. Dincer, M. Agelin-Chaab, R. Fraser, and M. Fowler, "Experimental and theoretical investigation of temperature distributions in a prismatic lithium-ion battery," International Journal of Thermal Sciences, vol. 99, pp. 204–212, 2016. doi: https://doi.org/10.1016/j.ijthermalsci.2015.08.016

[2] S. Panchal, I. Dincer, M. Agelin-Chaab, R. Fraser, and M. Fowler, "Experimental and theoretical investigations of heat generation rates for a water cooled LiFePO4 battery," Int J Heat Mass Transf, vol. 101, pp. 1093–1102, 2016. doi: https://doi.org/10.1016/j.ijheatmasstransfer.2016.05.126

[3] T. Yang, N. Yang, X. Zhang, and G. Li, "Investigation of the thermal performance of axial-flow air cooling for the lithium-ion battery pack," International Journal of Thermal Sciences, vol. 108, pp. 132–144, 2016. doi: https://doi.org/10.1016/j.ijthermalsci.2016.05.009

[4] A. Greco, X. Jiang, and D. Cao, "An investigation of lithium-ion battery thermal management using paraffin/porous-graphite-matrix composite," J Power Sources, vol. 278, pp. 50–68, 2015. doi: https://doi.org/10.1016/j.jpowsour.2014.12.027

[5] L. Luo, Y. Liu, Z. Liao, and J. Zhong, "Optimal structure design and heat transfer characteristic analysis of X- type air-cooled battery thermal management system," J Energy Storage, vol. 67, p. 107681, 2023. doi: https://doi.org/10.1016/j.est.2023.107681

[6] G. Mohammed, H. Hasini, K. E. Elfeky, Q. Wang, M. A. Hajara, and N. I. Om, "Cooling effectiveness enhancement of parallel air-cooled battery system through integration with multi-phase change materials," International Journal of Thermal Sciences, vol. 201, p. 109030, 2024. doi: https://doi.org/10.1016/j.ijthermalsci.2024.109030

[7] W. Liang et al., "Optimization design of proton exchange membrane fuel cell cooling plate based on dual- objective function topology theory," International Communications in Heat and Mass Transfer, vol. 153, p. 107404, 2024. doi: https://doi.org/10.1016/j.icheatmasstransfer.2024.107404

[8] Q. Xu et al., "Enhancement of thermal management for cylindrical battery module based on a novel wrench- shaped design for the cold plate," Sustainable Energy Technologies and Assessments, vol. 59, p. 103421, 2023.

[9] M. Zheng et al., "Numerical study on power battery thermal management system based on heat pipe technology," Energy Reports, vol. 9, pp. 350–361, 2023. doi: https://doi.org/10.1016/j.seta.2023.103421

[10] J. Wang, Y. Gan, J. Liang, M. Tan, and Y. Li, "Sensitivity analysis of factors influencing a heat pipe-based thermal management system for a battery module with cylindrical cells," Appl Therm Eng, vol. 151, pp. 475– 485, 2019. doi: https://doi.org/10.1016/j.applthermaleng.2019.02.036

[11] S. Mousavi, A. Zadehkabir, M. Siavashi, and X. Yang, "An improved hybrid thermal management system for prismatic Li-ion batteries integrated with mini-channel and phase change materials," Appl Energy, vol. 334, p. 120643, 2023. doi: https://doi.org/10.1016/j.apenergy.2023.120643
[12] Z. Liu, C. Huadan, B. Wang, and P. Li, "Coupling optimization of protruding fin and PCM in hybrid cooling system and cycle strategy matching for lithium-ion battery thermal management," International Journal of Thermal Sciences, vol. 207, p. 109372, 2025. doi: https://doi.org/10.1016/j.ijthermalsci.2024.109372
[13] L. Rong, X.-S. Bai, J.-C. Li, R.-Z. Zhang, and W.-W. Yang, "Design and optimization of a hybrid cooling configuration combining PCM and liquid cooling for Li-ion battery using data-based response surface approximation model," Appl Therm Eng, vol. 245, p. 122844, 2024. doi: https://doi.org/10.1016/j.applthermaleng.2024.122844
[14] H. Yang, G. Yang, N. Liu, S. Zhang, and Q. Gao, "Investigating the impact of inlet angle on the performance of air-cooling lithium-ion battery pack," Appl Therm Eng, vol. 263, p. 125314, 2025. doi: https://doi.org/10.1016/j.applthermaleng.2024.125314
[15] W. Wu, S. Wang, W. Wu, K. Chen, S. Hong, and Y. Lai, "A critical review of battery thermal performance and liquid based battery thermal management," Energy Convers Manag, vol. 182, pp. 262–281, 2019. doi: https://doi.org/10.1016/j.enconman.2018.12.051
[16] Wu et al., "A review on the liquid cooling thermal management system of lithium-ion batteries," Appl Energy, vol. 375, p. 124173, 2024. doi: https://doi.org/10.1016/j.apenergy.2024.124173
[17] S. M. A. Aftab, A. S. Mohd Rafie, N. A. Razak, and K. A. Ahmad, "Turbulence model selection for low Reynolds number flows," PLoS One, vol. 11, no. 4, p. e0153755, 2016. doi: https://doi.org/10.1371/journal.pone.0153755
[18] Zhang and K. Wei, "Experimental and numerical study of a passive thermal management system using flat heat pipes for lithium-ion batteries," Appl Therm Eng, vol. 166, p. 114660, 2020. doi: https://doi.org/10.1016/j.applthermaleng.2019.114660
[19] C. Wang et al., "Liquid cooling based on thermal silica plate for battery thermal management system," Int J Energy Res, vol. 41, no. 15, pp. 2468–2479, 2017. doi: https://doi.org/10.1002/er.3801
[20] Z. Wang, J. Ma, and L. Zhang, "Finite element thermal model and simulation for a cylindrical Li-ion battery," IEEE Access, vol. 5, pp. 15372–15379, 2017. doi: 10.1109/ACCESS.2017.2723436
[21] X. Peng, C. Ma, A. Garg, N. Bao, and X. Liao, "Thermal performance investigation of an air-cooled lithium-ion battery pack considering the inconsistency of battery cells," Appl Therm Eng, vol. 153, pp. 596–603, 2019. doi: https://doi.org/10.1016/j.applthermaleng.2019.03.042
[22] P. J. Roache, "Perspective: a method for uniform reporting of grid refinement studies," 1994. doi: https://doi.org/10.1115/1.2910291
[23] Rao, Y. Huo, X. Liu, and G. Zhang, "Experimental investigation of battery thermal management system for electric vehicle based on paraffin/copper foam," Journal of the Energy Institute, vol. 88, no. 3, pp. 241–246, 2015. doi: https://doi.org/10.1016/j.joei.2014.09.006